Supercritical Burning of Liquid Oxygen (LOX) Droplet with Detailed Chemistry

J. DAOU,* P. HALDENWANG, and C. NICOLI

Laboratoire de Recherche en Combustion, URA-CNRS 1117, Université de Provence, Centre de St-Jerome, Service 252, (F) 13397 Marseille CEDEX 20, France

A numerical study of the supercritical combustion of a liquid oxygen (LOX) droplet in a stagnant environment of hot hydrogen is carried out with a detailed chemistry model. Special attention is devoted to ignition process and diffusion flame structure. Ignition consists typically of the propagation of a premixed flame which is initiated in the H_2-rich hot side. Propagation takes place in a nonhomogeneous hot environment (say 1500 K) with a considerable velocity (typically 50 ms^{-1}). Despite the high temperature of the ambiance, the medium ahead of the flame can be considered as frozen during the transit time. In addition, it is found that droplets with diameter less than 1 μm vaporize before burning. A quasi-steady-like diffusion flame is then established. In this regime we observe that the D^2 law is approximately valid. In contrast to the case of a single irreversible reaction, a full chemistry model leads to a very thick flame where chemical consumption and production cover a surrounding zone about four times the instantaneous droplet radius. Reversibility of the reactions plays a determinant role in the flame structure by inducing a large near-equilibrium zone which is separated from a frozen region by a thin nonequilibrium zone. The length scale of the latter region is found to behave as the square root of the instantaneous droplet radius and a detailed analysis shows that just two elementary reactions are involved in this zone. Furthermore, the influence of several parameters is considered; temperature and pressure in the combustion chamber have a weak influence on the burning time. Influence of initial droplet radius confirms that droplet combustion is a diffusion controlled process. Chamber composition is also considered. Finally, it is shown that a precise description of the transport properties in the dense phase is not required.

INTRODUCTION

High-pressure droplet vaporization and combustion have received significant attention lately. This is mainly due to the need of a deeper understanding in this subject area for the development of high-pressure combustion devices such as liquid-propellant rocket motors and diesel engines.

It is well established [1, 2] that, when the ambient pressure exceeds the critical pressure of one of the droplet components, the droplet liquid–vapor interface can disappear and the process has to be considered as the combustion of a "puff" of a dense fluid surrounded by a light one. The conditions under which such a supercritical regime is reached, have been the purpose of recent investigations [3–6].

In the present work we assume that these conditions are met as soon as the droplet is injected in the chamber. These conditions for LOX droplets could be attained for instance, as soon as water vapor is present in the chamber and the pressure is higher than the O_2 critical pressure (50 bars). This is supported by a thermodynamic study of liquid-vapor coexistence, briefly reported in Appendix.

Experiments with hydrocarbon droplet combustion by Faeth et al. [1] and Sato et al. [7] have shown the existence of the supercritical regime for combustion. They observed, above the critical pressure, a change in the dependency of the combustion time: it weakly increases with respect to pressure. Several theoretical approaches have been proposed within the framework of the flame sheet concept. Spalding [8] considered a dense pocket reduced to a point source, Rosner [9] extended this to a distributed source while Sanchez-Tarifa et al. [10] provided a solution using asymptotic matching. Shuen et al. [5] carried out a numerical study with a one-step irreversible chemical reaction, applied to n-pentane droplets.

The present paper specifically addresses the combustion of a LOX droplet in a high-pres-

*Corresponding author.

COMBUSTION AND FLAME 101: 153–169 (1995)

Published by Elsevier Science Inc.

0010-2180/95/$9.50
SSDI 0010-2180(94)00201-3

sure, hot hydrogen stagnant environment, with a detailed chemistry model [11] including 8 species and 37 elementary reactions. Although the absence of a reliable experimental confirmation makes it difficult to ascertain that any available chemical scheme is valid at high pressure ($\sim$ 100 bars), the use of a detailed mechanism provides a much better description of LOX droplet ignition and combustion than a simplified one step irreversible reaction. Among the realistic features captured: a realistic flame temperature as encountered in rocket engines ($\sim$ 4000 K), an important presence of radicals, a very thick flame resulting from reversibility effects... Moreover the fact that H_2–O_2 combustion is very fast—so that near-equilibrium prevails almost everywhere—makes most of our results (Quasi-steady profiles, combustion time, influence of chamber characteristics) less sensitive to chemical kinetics. Because we are particularly interested in flame description, we have used gas phase thermodynamic and transport properties. Such a practice is questionable for the dense fluid (i.e., the "droplet" and its close vicinity): we will show nevertheless on a typical example that the use of more sophisticated modelling for dense phase properties would have a negligible influence as long as the density is correctly estimated in the dense phase. This is the reason why we have systematically used the Redlich-Kwong-Soave equation of state for high-pressure mixture.

The paper is organized as follows.

In the first section we present the problem to be solved with numerics: the single-phase conservation equations written in spherical geometry, the transport and thermodynamic model used and the finite volume numerical scheme.

The second part provides the numerical results for ignition. After extracting some orders of magnitude from the study of the homogeneous case, the actual ignition of a LOX droplet is described. The influence of initial droplet radius is investigated.

In the third part, we follow the whole temporal evolution of the droplet burning. A steady-combustion-like regime is observed for sufficiently large droplets and we check the validity of the related classical results. Then a detailed analysis of the diffusion flame structure is carried out. Finally, the influence of some relevant parameters on combustion time is investigated.

THE MODEL

The ignition and combustion of a LOX droplet in a high-pressure hot hydrogen environment is considered. The droplet is assumed to be in a supercritical state from the beginning. Just one phase is thus present, the "droplet" being the dense cold region around the origin. The droplet interface can be defined as the locus where either temperature, density, or oxygen mass fraction has an initially prescribed value (close to those of the origin). The influence of this choice will be discussed later: as a matter of fact, these three possible definitions are nearly equivalent in predicting droplet lifetimes, except for small droplets where important differences are noted.

Equations

The mass and energy conservation equations to be solved in spherical geometry are the following:

$$\frac{\partial \rho}{\partial t} + \frac{1}{r^2}\frac{\partial}{\partial r}(r^2 \rho v) = 0, \tag{1}$$

$$\rho \frac{\partial Y_k}{\partial t} + \rho v \frac{\partial Y_k}{\partial r} = -\frac{1}{r^2}\frac{\partial}{\partial r}(r^2 J_k) + \dot{\omega}_k W_k, \qquad k = 1,8, \tag{2}$$

$$\rho c_p \frac{\partial T}{\partial t} + \rho v c_p \frac{\partial T}{\partial r} = \frac{1}{r^2}\frac{\partial}{\partial r}\left(r^2 \lambda \frac{\partial T}{\partial r}\right) - \sum_{k=1}^{8} c_{pk} J_k \frac{\partial T}{\partial r} - \sum_{k=1}^{8} h_k \dot{\omega}_k W_k \tag{3}$$

where T is the temperature and Y_k are the mass fractions of the eight species involved. They are respectively: H_2–O_2–H–O–OH–HO_2–H_2O–H_2O_2.

ρ is the mass density, c_p the mass weighted mean specific heat at constant pressure, h_k the specific enthalpies of the species, w_k the molar

production rates of the species, and W_k the molecular weights of the species. J_k is the diffusive flux of species k. Modeling of all these physical quantities are presented in the next paragraph.

The boundary conditions are:

—zero gradients at $r = 0$ for all dependent variables (T, Y_k, $k = 1 \ldots 8$) due to the spherical geometry
—prescribed values at infinity for the dependent variables. Infinity is numerically at hundred initial droplet radii from the origin.

The initial conditions:

For all quantities, piecewise linear profiles are prescribed by specifying the values at the origin, at the initial "interface" located at a_0 and at infinity. Thus, the dependent variable fields are essentially uniform from $r = 0$ to $r \sim a_0$ and from $r \sim a_0$ to infinity. A transition zone around a_0 is numerically necessary, its thickness is taken of the order of $0.01\ a_0$.

Equation of State, Transport, and Thermodynamic Properties

The Redlich–Kwong–Soave equation of state is used to define the density field as a function of temperature, pressure and composition. For a single component i this equation reads

$$P = \frac{RT}{V - b_i} - \frac{a_i}{V(V + b_i)},$$

where a_i and b_i depend on the critical temperature and pressure of this component [12, 13]. The coefficient a_i also includes an empirical simple function of ω, the acentric factor which is an experimental data ($\omega = -\log[P_{\text{sat}}/P_c]$ where P_{sat} is the saturation pressure at $T = 0.7{*}T_c$ and T_c the critical pressure). The same form of equation of state is extended to mixtures when a_i and b_i are replaced by a_m and b_m defined by simple mixing rules: $a_m^{1/2} = \Sigma x_i a_i^{1/2}$ and $b_m = \Sigma x_i b_i$ (x_i: mole fraction of component i). Although this practice is essentially empirical, it has received a large experimental support [12, 13].

A slight difficulty arises in our case due to the presence of radicals and metastable species for which those coefficients can not be defined. To circumvent this difficulty, just the three main species H_2, O_2, and H_2O are considered when using this equation (i.e. their mole fractions are normalized so that they sum up to unity). The error occasioned by this practice is negligible because the sum of the mole fractions of these species deviates significantly from one only in high temperature regions (due to a significant presence of radicals) and in this case the equation of state is equivalent to the perfect gas law.

Thermochemical and transport properties are evaluated using the gas-phase packages—CHEMKIN [14] and TRANSPORT [15]. These properties are temperature dependent and functions of the mixture composition through averaging formula. The thermal conductivity is independent of pressure and the diffusion coefficients are inversely proportional to pressure. A nonzero thermal diffusion velocity is included for the low molecular weight species (H and H_2) in the evaluation of J_k, the diffusive fluxes.

The use of the same expressions (from gaseous origin) throughout the domain, enables a continuous spatial variation of the transport and thermodynamic properties, which is an expected feature of a supercritical fluid. However this use is of course questionable and certainly incorrect in the dense (liquidlike) phase. However it turns out, as shown on a typical example given below, that the influence of the transport properties of the dense phase plays a negligible role on the total burning time. This conclusion is in complete agreement with the expression of the combustion time yielded by the analytical study by Sanchez-Tarifa et al. [10]. A similar conclusion about the weak sensitivity of droplet lifetime to transport coefficients in the dense phase has been also drawn in the numerical study by Curtis et al. [16].

Let us indicate here that the modelling presented above seems satisfactory, although a more sophisticated one might be partly possible. Because of the large uncertainties associated with the transport property estimation methods for dense mixtures [12], and because of the simultaneous presence of a large number of delicate issues in our problem (the disappearance of the interface suggested by our

thermodynamic study (cf Appendix), the evaluation of diffusion coefficients, the important concentrations of radicals and metastable species, the polarity of H_2O, the chemical kinetics...), it is not recommended to seek high accuracy in some cases while this can not be achieved in others. This remark applies for instance to the modification of the equation of state to take account of "the quantum effects" of H_2 as in [4]; such a practice would change our results by less than 1%.

The Numerical Method

Equations 1–3 are discretized using a finite-volume approach [17] and solved in two steps [18].

—A reaction step where only the transient term is kept at the left-hand sides of Eqs. 2–3 and the chemical term is kept at the right-hand side. The resulting stiff system of ordinary differential equations is solved using LSODE solver [19]. This first step allows deduction of an averaged value of the chemical source terms over the time step at each grid point

—A reaction-convection-diffusion step where the whole system is solved implicitly with the chemical source term being replaced by its averaged value from the first step. An upwind discretization is applied to the convective term.

The space grid is not uniform but fixed in time. Three quarters of the grid points lay within 6 initial radii from the origin, the rest being used to cover the remaining domain. The number of grid points used varies from 200 to 1500.

RESULTS AND DISCUSSION

In this section we begin with a quick analysis of the homogeneous case. This is done in order to determine some orders of magnitude needed to interpret subsequent results. The actual ignition process is then studied and the history of a LOX droplet burning in hydrogen is described. A quasi-steady-like regime can be observed. Finally, the influence of some parameters on combustion time is briefly discussed.

The Homogeneous Case

It is of particular interest to describe the chemical equilibrium related to the homogeneous adiabatic combustion of a O_2/H_2 mixture. Three points are considered: ignition delay, adiabatic flame temperature and equilibrium composition.

The ignition delay depends on pressure, initial temperature, and initial composition of the reactive mixture. We will choose a typical pressure of 100 bars, and determine the effect of initial dilution with H_2O, and the influence of H_2/O_2 ratio. Equations 2–3 are solved with the space derivatives removed and with different initial conditions. The induction delay is defined as the inflection point of T versus time.

As a typical example, the influence of H_2/O_2 equivalence ratio on induction delay for a nondiluted O_2–H_2 mixture at 100 bars and 1500 K is illustrated by Table 1:

In order to take into account the presence of radicals at high temperature in a real combustion chamber some of the calculations below were carried out with an initial mole fraction of the radical H equal to 10^{-3}. This choice is not arbitrary, and corresponds to the composition of this radical in equilibrium with H_2 at high temperature, typically at 2000 K. As a result, the ignition delay is shortened as seen on Table 2 where ignition delay and adiabatic flame temperature for a stoichiometric mixture at 100 bars and 1500 K are given as a function of the initial H_2O mole fraction.

The influence of initial temperature and pressure on the adiabatic flame temperature is illustrated in Fig. 1, where the adiabatic flame temperature is plotted versus pressure for four initial temperatures between 1000 and 2500 K.

The equilibrium temperature and composition of an initial stoichiometric nondiluted mixture at 100 bars and 1500 K (case 1 in

TABLE 1

H_2/O_2 equation ratio	0.5	1	2	5	10
Induction delay/(μs)	1.63	1.46	1.40	1.44	1.57

TABLE 2

XH_2O	0	0.25	0.5
Ignition delay (μs)	.37	1.2	2.3
Adiabatic flame temp (K)	3993	3576	3065

Table 2) are the following:

$T = 3993$ K. $XH_2 = 0.16$,
$XO_2 = 0.04$,
$XH_2O = 0.56$,
$XH = 0.06$,
$XO = 0.03$,
$XOH = 0.15$,
$XHO_2 = 0.21\ 10^{-3}$
$XH_2O_2 = 0.5\ 10^{-4}$.

A rapid glance at the equilibrium composition shows that the reactants are not totally depleted and thus the importance of reversibility effects. The concentration of radicals is very important, OH being the predominant one. These results for a homogeneous flame indicates that the diffusion flame around a droplet will present an important feature: the reversible effects will lead to the broadening of the flame [20–21].

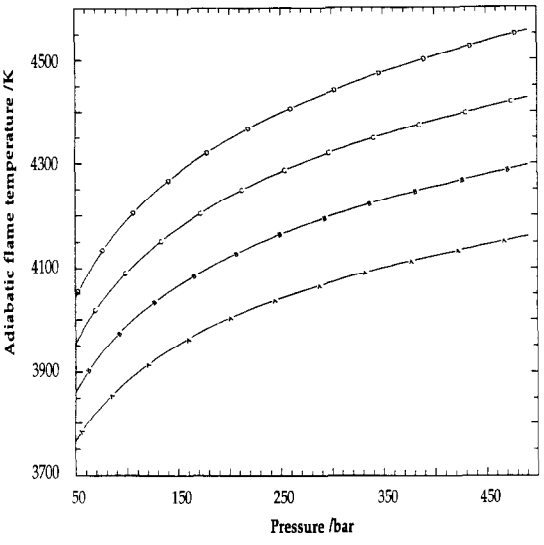

Fig. 1. Flame temperature versus pressure of a stoichiometric H_2/O_2 mixture for four initial temperatures (Curve A $T = 1000$ K, Curve B $T = 1500$ K, Curve C $T = 2000$ K, Curve D $T = 2500$ K).

Ignition of a LOX Droplet in a Hot Hydrogen Environment

The actual ignition occurs in a non homogeneous medium and depends on the mechanical time (convection-diffusion) involved, which in turn depends on droplet radius. The influence of droplet radius on ignition is addressed in the next paragraph while here we describe the ignition process in a typical case.

Now we solve the complete set of Eqs. 1–3 with the boundary conditions already mentioned. The initial conditions are the following: the initial "interface" is located at $r = a_0$. The initial profiles are uniform for $r < a_0$ and for $r > 1.02a_0$, and linear between a_0 and $1.02a_0$. As a typical example, the initially prescribed values "in the droplet" (i.e., $r < a_0$) denoted with the superscript 0, and in the ambiance ($r > 1.02a_0$) denoted with the superscript ∞, for the case to be considered in this paragraph are

$$X_{O_2}^{\ 0} = 1 \quad X_{O_2}^{\ \infty} = 0; \quad X_{H_2}^{\ 0} = 0 \quad X_{H_2}^{\ \infty} = 1;$$

$$T^0 = 90 \text{ K}; \quad T^\infty = 1500 \text{ K}.$$

The initial mole fractions of the other species are zero, and $a_0 = 20$ μm. The ambient pressure is 100 bars.

Let us describe the ignition process. Figure 2 shows the temperature profile at five instants, namely 2.8, 2.9, 3.0, 3.1, and 3.2 μs. It is seen that the initial runaway occurs in the H_2-rich side, and that a steep thermal front propagates towards the droplet in an increasingly lean and cold mixture. In what follows we will confirm that this front represents a deflagration wave accompanying the installation of a diffusion flame. It is expected [22] to consume the deficient reactant on its way towards the droplet, leaving a diffusion flame after it crosses the stoichiometric point.

In Fig. 3 we notice that the ignition time in the nonhomogeneous case is about twice the homogeneous one which is indicated in Table 1. This delay obviously includes an initial mixing time. The heat release accompanying the premixed flame propagation is illustrated in Fig. 4 which represents five instantaneous heat rate profiles, at the same instants as in Fig. 2. The ignition starts in a point located around

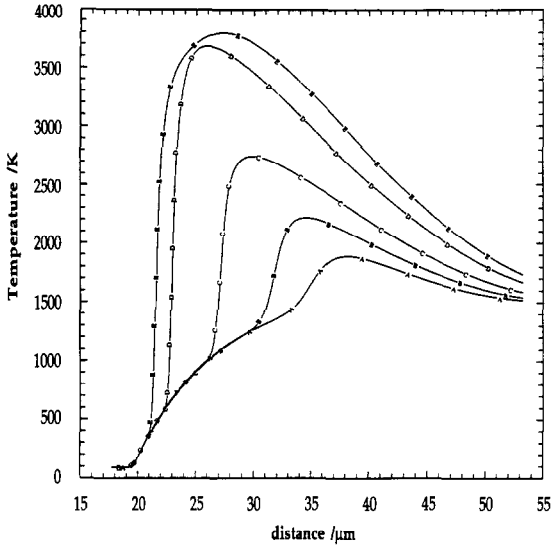

Fig. 2. Temperature profiles during the ignition of a 20-μm-radius droplet at 90 K in a hot hydrogen gas at 1500 K and 100 bars. Curve A—time = 2.8 μs; B—t = 2.9 μs; C—t = 3.0 μs; D—t = 3.1 μs; E—t = 3.2 μs.

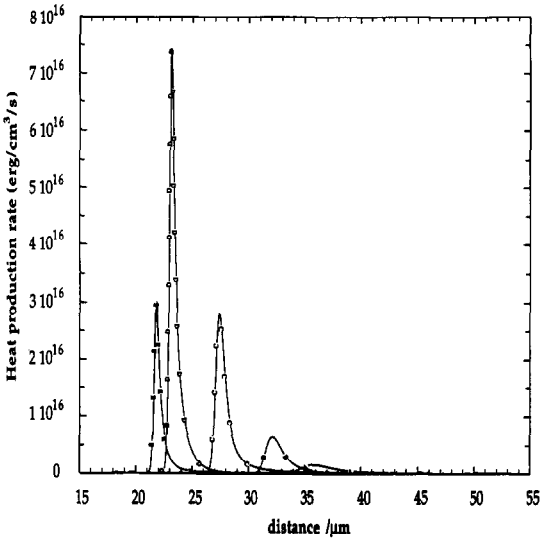

Fig. 4. Heat production profiles during the ignition of a 20-μm-radius droplet at 90 K in a hot hydrogen gas at 1500 K and 100 bars. Curve A—time = 2.8 μs; B—t = 2.9 μs; C—t = 3.0 μs; D—t = 3.1 μs; E—t = 3.2 μs.

$2a_0$. The heat production peak increases then decreases. We have followed in time the position of this peak and deduced its velocity which is shown in Fig. 5. This front speeds up as long as the equivalence ratio decreases to 1. When the stoichiometric point is reached the front begins to slow down and finally vanishes in the close vicinity of the droplet. As for the intensity of the velocity, it is quite unusual to notice that the maximum in Fig. 5 is around 50 m/s. This point will be discussed below.

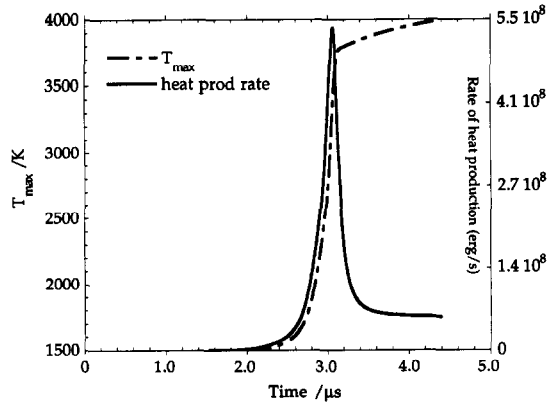

Fig. 3. Maximum temperature and total heat production rate versus time during the ignition of a 20-μm-radius droplet at 90 K in a hot hydrogen gas at 1500 K and 100 bars.

An interesting question to be raised here is about the nature of the thermal front encountered. Its propagation takes place in a hot premixed environment, and it is legitimate to ask whether this wave is a deflagration. More precisely, can the medium ahead of the flame be considered as chemically frozen during the

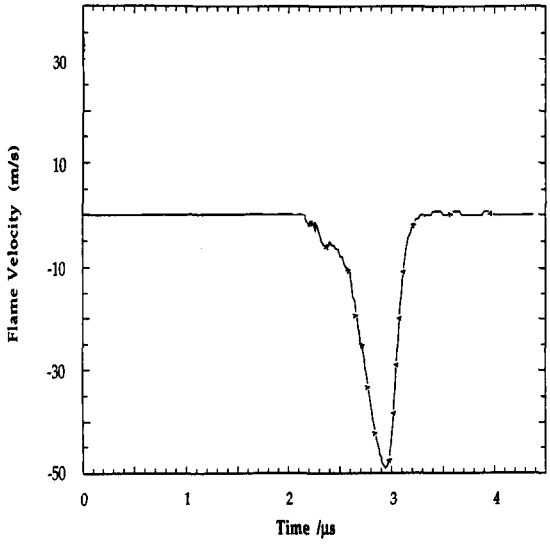

Fig. 5. Velocity of the premixed flame, defined as the velocity of the maximum of the heat production rate, during the ignition of a 20-μm-radius droplet at 90 K in a hot hydrogen gas at 1500 K and 100 bars.

transit time? First let us consider the most energetic stage of this reactive wave. This corresponds approximately to curve D in Fig. 4. At this instant we can investigate the balance between reaction, diffusion, advection processes as follows. Considering the major terms in Equation (3) and rewriting it as

$$A + B + C + D \sim 0,$$

where

$$A = \rho v \frac{\partial T}{\partial r}, \quad B = \frac{-1}{c_p r^2} \frac{\partial}{\partial r}\left(r^2 \lambda \frac{\partial T}{\partial r}\right),$$

$$C = \frac{-1}{c_p} \sum_{k=1}^{8} h_k \dot{\omega}_k W_k, \quad D = \rho \frac{\partial T}{\partial t}$$

A, B, C, and D represent respectively the advection, diffusion, reaction and transient terms. The radial profile of these four quantities are plotted in Fig. 6 which is in fact a zoom from $r = 21.2$ μm to $r = 24.8$ μm. It is seen that ahead of the wave the chemical term (C) is practically zero, so that the transient term (D) is only due to heat conduction (B). The wave is consequently a deflagration. As a matter of fact, it can be shown that rapid deflagration waves exist in O_2–H_2 mixtures at high temperatures (> 1000 K), but only at high pressure [23]. Finally, note that the flame thickness in our present case is about 2 μm. This scale can be considered as the typical reaction-diffusion length.

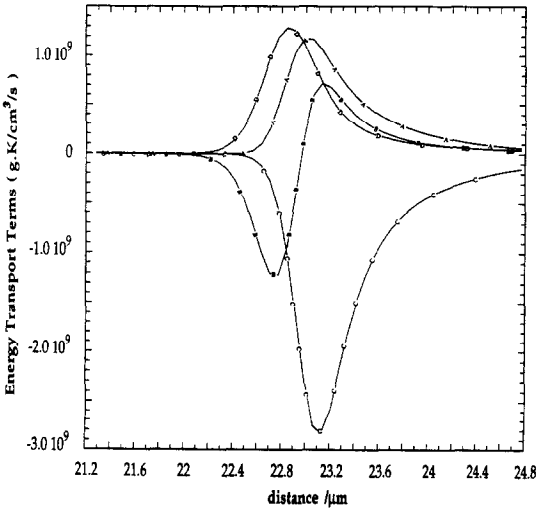

Fig. 6. Dominant terms of the energy equation versus space. A represents the convective term, B the diffusive Fourier term, C the energy source term, D the transient term (divided by Cp) as they appear when they are in the left hand side of Eq. 3.

Influence of Droplet Radius on Ignition Delay

The aim of this paragraph is to study more quantitatively the influence of droplet radius on combustion delay. It is expected that a significant increase in combustion delay will occur when the mechanical time (convective or diffusive) decreases until it becomes of the same order of magnitude as the homogeneous induction time. As a typical example at $p = 100$ bars for an ambient temperature of 1500 K and an initial mole fraction of H-radical of 10^{-3}, the induction time (as quoted on Table 2) is about 0.3 μs. The thermal diffusion coefficient D_{th} in the ambient gas being about 0.5 cm^2/s, the diffusion time a_0^2/D_{th} becomes comparable to the induction time for $a_0 \sim 4$ μm. As shown in Table 3, the increase of the induction time becomes significant for radii smaller than 5 μm, and small droplets with radii around 1 μm are expected to disappear before burning.

History and Characterization of a Burning Droplet

In this paragraph we follow the temporal evolution of a droplet until its disappearance. As a typical example, a 50 μm-radius droplet burning in hydrogen at 1500 K and 100 bars is considered. The initial temperature of the droplet is 90 K, and an initial mole fraction of 10^{-3} is assumed for H-radical in the ambiance. This example is also the opportunity to precisely define the droplet combustion time and

TABLE 3

Droplet radius (μm)	50	10	5	2	1	0.5
Induction time (μs) (ambient temp. = 1500 K)	0.65	0.7	0.98	1.6	greater than lifetime	

to compare the three definitions adopted for the instantaneous droplet radius:

—the locus where the oxygen mole fraction is equal to 0.99.
—the locus where the temperature is equal to 91 K.
—the locus where the density is equal to its initial value at the interface.

Figure 7 shows the evolution of the droplet radius defined with respect to these three definitions. It is noticed that the estimate of the instantaneous radius, and especially the droplet lifetime is not very sensitive to the choice of one of those definitions. Nevertheless, at the beginning (i.e., before ignition), a discrepancy between these definitions is noted.

The issue of the choice of the droplet radius definition is more serious in super-critical vaporization without combustion [6] because all fields can diffuse quasi-independently: they are not coupled by combustion.

As for the burning time determination in the context of supercritical combustion, we have selected a relevant quantity which is independent of a precise definition of the interface: the total mass of oxygen (integrated over space), plotted in Fig. 7. It is seen to vanish almost simultaneously with the radii presented on the same figure, in a time close to 1.1 ms.

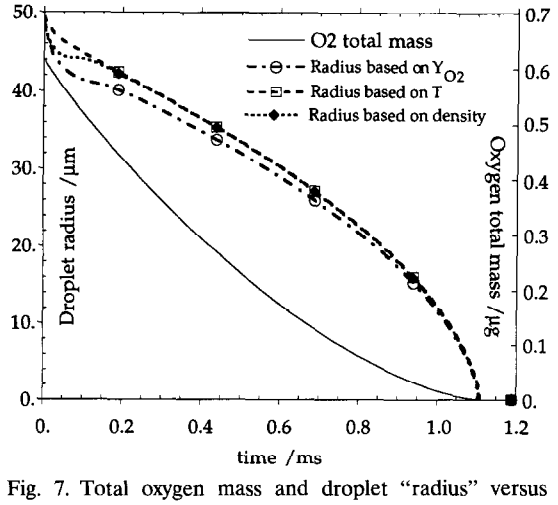

Fig. 7. Total oxygen mass and droplet "radius" versus time, for a 50-μm-radius droplet at 90 K in a hot hydrogen gas at 1500 K and 100 bars. The definition of the radius is based on a particular value of oxygen mole fraction (Curve A), temperature field (Curve B) or density field (Curve C).

The combustion time used below will be defined as the time needed for the oxygen mass to vanish.

At this point, it is interesting to check how far the classical results of the quasi-steady theory apply. First, concerning the D^2 law, we plot in Fig. 8 the square of the droplet radius (based on T). After a transient time close to 0.15 ms, it is seen that this law is approximately satisfied during almost the entire combustion time. The quasi-steady theory finds another confirmation on the same figure where the maximum temperature is plotted. After the same transient time mentioned, this maximum reaches a peak value close to 4250 K, which can be considered as stationary during most of the combustion time. On the other hand, if we plot in Fig. 9 more sensitive quantities like the ratio of the maximum-temperature locus over the instantaneous droplet radius (Curve B) or the maximum-heat release locus over instantaneous droplet radius (Curve A), it turns out that the quasi-steady regime can never be considered as completely established, these ratios being an increasing function of time. It is interesting to note that the maximum heat release is located very close to the droplet interface (within half a droplet radius). This point will be discussed in the next paragraph.

Structure of the Established Diffusion Flame

After ignition, a quasi-steady like regime is established during which the D^2 law is approximately valid and the flame temperature con-

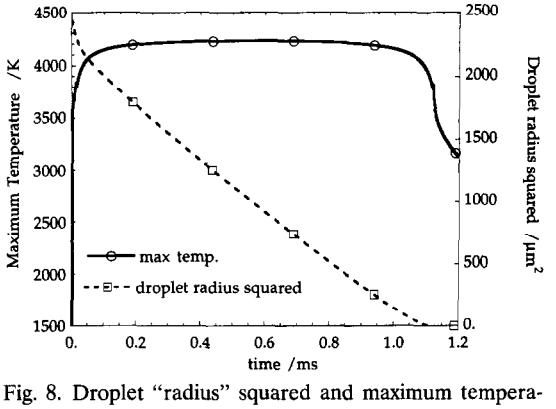

Fig. 8. Droplet "radius" squared and maximum temperature versus time, for a 50-μm-radius droplet at 90 K in a hot hydrogen gas at 1500 K and 100 bars.

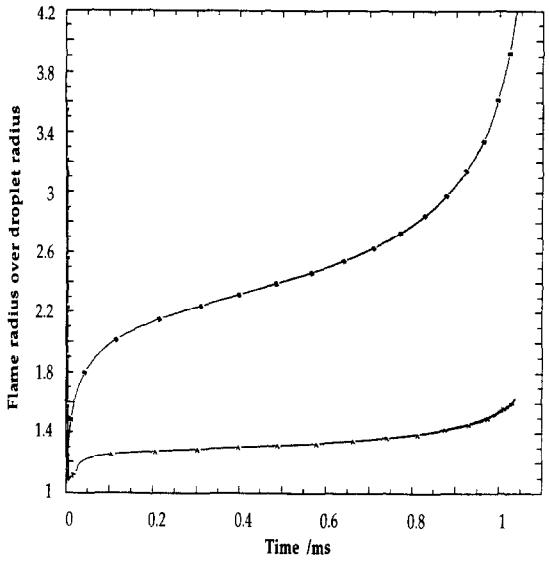

Fig. 9. Ratio of the radius of the heat production rate maximum over droplet radius (Curve A), and ratio of the radius of the maximum temperature over droplet radius (Curve B) versus time, for a 50-μm-radius droplet at 90 K in a hot hydrogen gas at 1500 K and 100 bars.

stant, as seen in the previous paragraph. We study now in detail the diffusion flame that presents many differences with the flame sheet model or a single reaction irreversible model. As will be shown, the flame is indeed very thick with a chemistry in near equilibrium, with production and consumption zones covering large domains. Let us return to the case studied previously: a 50-μm radius droplet burning in a chamber characterized by an ambient gas at 100 bars and 1500 K.

After a transient regime of the order of some diffusion times (say 0.2 ms), the maximum flame temperature is reached and a flame structure, which at first glance looks self-similar, accompanies the droplet regression. Let us describe temperature, density, and velocity profiles (plotted in Fig. 10) when the droplet radius is about 40 μm (i.e., at $t = 0.3$ ms). The temperature profile presents a maximum close to 4250 K located at about 2.3 times the instantaneous radius. This flame temperature is higher than in the homogeneous case where it is about 4000 K. This is classically explained [24] by nonunity Lewis number, which is typical of hydrogen flames. The density profile separates clearly a dense region from a light one, the transition from the first one with a typical

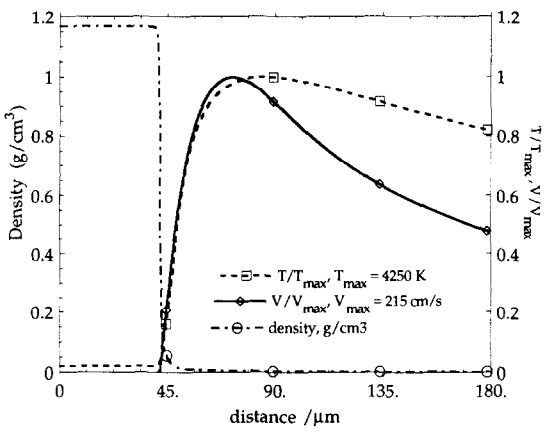

Fig. 10. Temperature, velocity and density profiles at $t = 0.3$ ms, for a 50-μm-radius droplet at 90 K in a hot hydrogen gas at 1500 K and 100 bars.

density of 1.2 g/cm^3 to the second one with a density of 0.0012 g/cm^3 in the far field being very sharp. This steep density gradient is due to the temperature gradient amplified by a strong dependency of the equation of state on temperature in the vicinity of the dense phase. The difference in molecular weights between the droplet component and the ambiance acts in fact at a further distance from the droplet. The shape of the velocity profile is determined by the Stefan flow due to "vaporization" and by the gas expansion through the flame. In the far field the r^{-2} decrease is noticeable.

The mole fractions of the different species are presented in Fig. 11. Curve A that represents H_2 mole fraction, indicates that H_2 diffuses until a close vicinity of the droplet. On Curve B, relative to O_2, we observe that the droplet remains almost pure, and that oxygen is totally consumed by the reaction within three instantaneous droplet radii. Curve C presents the mole fraction of H-radical. Due to its high mobility, it diffuses within tens of radius away from the flame. Curves D and E are relative to O and OH-radicals. We note the importance already mentioned in the homogeneous case of OH-radical. The mole fractions of the metastable species HO_2 and H_2O_2 have been multiplied by 100 in order to be visible (curves F and H). HO_2 is however of capital importance for the heat generation as it will be shown below. Curve G is relative to H_2O.

The net production rates profiles, corresponding to the above species, are shown in

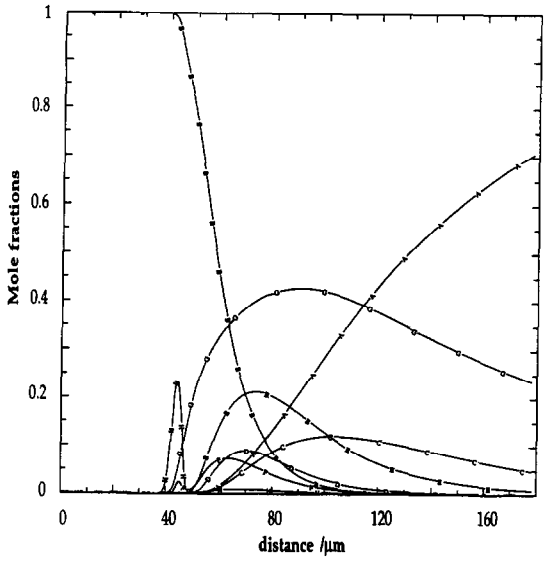

Fig. 11. Mole fractions profiles at $t = 0.3$ ms, for a 50-μm-radius droplet at 90 K in a hot hydrogen gas at 1500 K and 100 bars. A, B, C, D, E, F, G, H represent, respectively, H_2, O_2, H, O, OH, HO_2, H_2O, and H_2O_2 mole fractions (multiplied by 100 for HO_2 and H_2O_2).

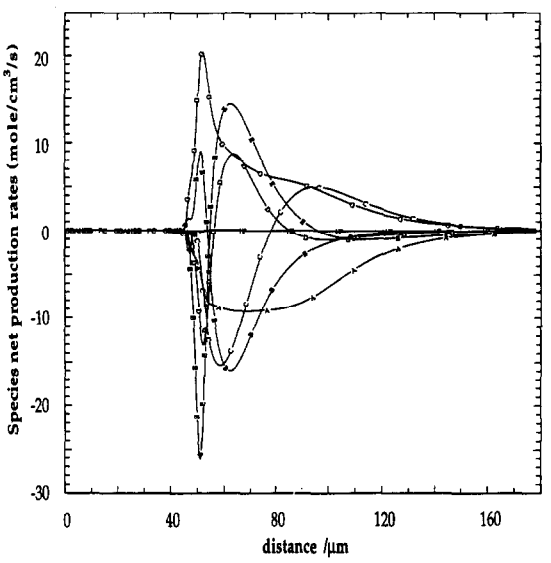

Fig. 12. Net production rates profiles at $t = 0.3$ ms, for a 50-μm-radius droplet at 90 K in a hot hydrogen gas at 1500 K and 100 bars. A, B, C, D, E, F, G, and H are relative, respectively, to H_2, O_2, H, O, OH, HO_2, H_2O, and H_2O_2.

Fig. 12 denoted with the same symbols as in Fig. 11. First we observe that the region of chemical activity covers a large zone from 46 to 160 μm. Second a thin region, with specific chemical activity, is noticeable in the vicinity of the droplet. It corresponds to a peak of H_2O net production (Curve G), peaks of O and OH net consumption (Curve D and E), and more surprisingly to a peak of O_2 net production. The heat production rate is plotted in Fig. 13 and it is observed to peak in this same narrow region.

To understand from a chemical point of view the existence of this thin region we have plotted in Fig. 14 the net rates of progress profiles of all the reactions (19 curves). The picture thus obtained is rather simple: just six reactions have a non negligible net contribution. Those are

$O_2 + H \leftrightarrow OH + O$ (Curve A)
$H_2 + O \leftrightarrow OH + H$ (Curve B)
$H_2 + OH \leftrightarrow H_2O + H$ (Curve C)
$OH + OH \leftrightarrow H_2O + O$ (Curve D)
$H + O_2 + M \leftrightarrow HO_2 + M$ (Curve H)
$HO_2 + OH \leftrightarrow H_2O + O_2$ (Curve M)

The last two recombination reactions are energetically the most important. They practically determine the heat production profile. The first one produces HO_2 and the second one consumes it, and their importance is due to the low activation energy of the direct reaction and the high exothermality (the latter implies high activation energy of the reverse reaction). This explains the existence of H_2O and heat production peaks near the interface where the temperature is low enough so that their reverse reactions can no longer keep pace with them. The net production rates of these two reactions are there, of the same order of magnitude of the forward rates and this narrow zone is in nonequilibrium. As for the O_2 production peak, its origin stems from the recombination of radicals (O and OH chain breaking) that have diffused to the cold region.

The region to the left of this narrow one can be considered as frozen because its chemical activity is very low. To the right-hand side of this transition domain, three reactions are predominant (illustrated by Curves B, C, and D in Fig. 14). Although they present net reaction rates larger than the ones of the transition zone (illustrated by Curves A, H, and M in Fig. 14) they do not play any energetic role for the

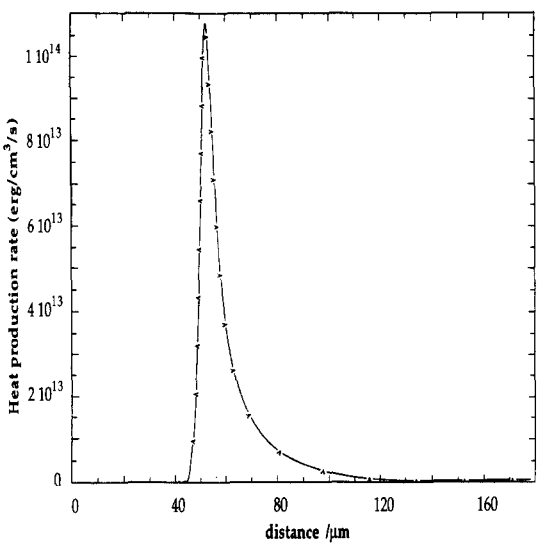

Fig. 13. Heat production rate profile at $t = 0.3$ ms, for a 50-μm-radius droplet at 90 K in a hot hydrogen gas at 1500 K and 100 bars.

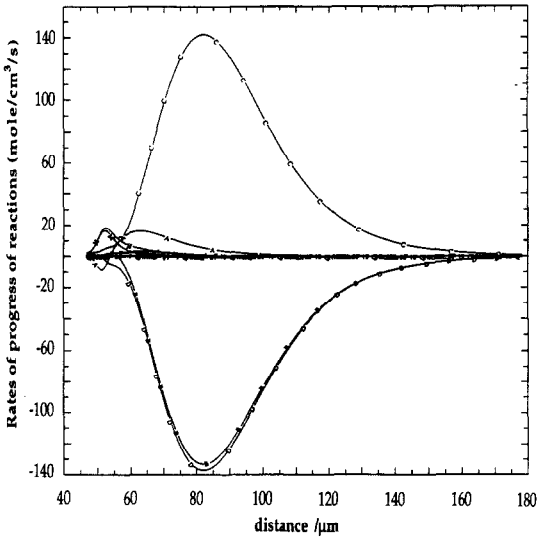

Fig. 14. Rates of progress of all reactions versus space. Just six reactions have a nonnegligible net contribution (CGS units):

$O_2 + H \leftrightarrow OH + O$	(Curve A)
$H_2 + O \leftrightarrow OH + H$	(Curve B)
$H_2 + OH \leftrightarrow H_2O + H$	(Curve C)
$OH + OH \leftrightarrow H_2O + O$	(CurveD)
$H + O_2 + M \leftrightarrow HO_2 + M$	(Curve H)
$HO_2 + OH \leftrightarrow H_2O + O_2$	(CurveM)

following reasons: C correspond to an exothermic process while D is related to an endothermic one of the same intensity, so that their global heat release remains negligible. As for the reaction represented by curve B, it is very weakly exothermal. In this region all the reactions can be considered in near equilibrium, that is the net rate of a reversible reaction is negligible compared to both the direct and the reverse rates as illustrated in Fig. 15 where Curve A [resp. B] represents the direct [resp. reverse] rate of progress of the reaction: $H + O_2 + M \leftrightarrow HO_2 + M$. We observe that the difference is not distinguishable. It is thus required to multiply the latter quantity by ten in order to make it appear as Curve C on Fig. 15.

Let us compare now the present diffusion flame with the simplified model by Linan [25] of a single irreversible reaction. In the framework of a single irreversible reaction, and assuming that the combustion is complete (i.e., no leakage occurs across the reaction zone), this coexistence zone is also the reaction zone with thickness l_R. If the reaction is fast, it is small compared with the diffusive length, which can be called the flame thickness l_F. More precisely, for a second-order reaction [25]

$$\frac{l_R}{l_F} \approx \mathrm{Da}^{-1/3}, \tag{4}$$

where Da is the Damköhler number that represents τ_m/τ_c, the ratio of the mechanical time by the chemical time. In droplet diffusion flames, the flame thickness is of the order of a, the droplet radius: $l_F \sim a$. The mechanical time is $\tau_m \sim a^2/D$. Equation 4 then rewrites

$$l_R \sim (D\tau_c)^{1/3} a^{1/3} \sim e^{2/3} a^{1/3}, \tag{5}$$

where $e = (D\tau_c)^{1/2}$ is an intrinsic diffusive-reactive length scale. Let us notice that ratio e/a is a infinitely small quantity as long as the droplet radius is larger than a few microns. Rewriting Eq. 5 as

$$\frac{l_R}{a} \approx \left(\frac{e}{a}\right)^{2/3}, \tag{6}$$

we conclude that l_R/a is a small quantity of lower order and that l_R is a new intermediate length scale resulting from the coupling be-

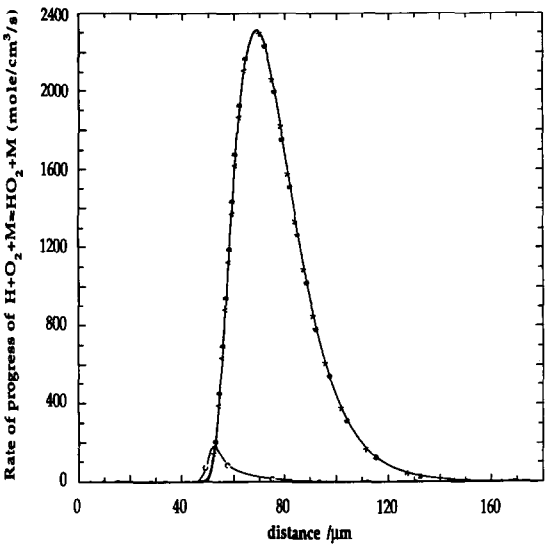

Fig. 15. Rate of progress of the reaction: $H + O_2 + M \leftrightarrow HO_2 + M$. Curve A [resp. B] represents the direct [resp. reverse] rate of progress. Curve C represents the net rate of progress multiplied by 10.

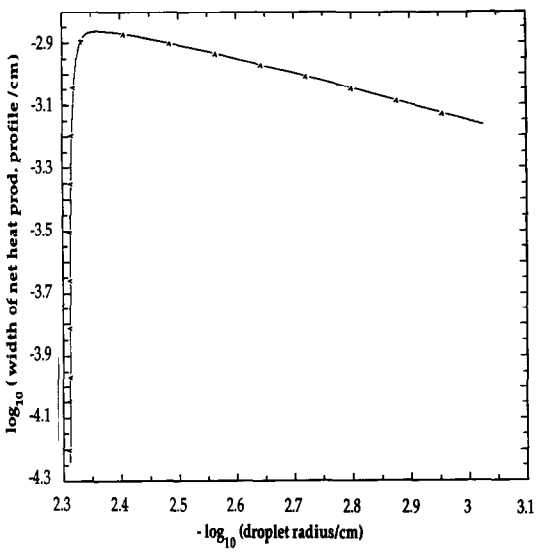

Fig. 16. Log_{10} (the width at half height of the net heat production rate profile) versus $-Log_{10}$ (instantaneous droplet radius).

tween both intrinsic ones: the instantaneous droplet radius and the reactive-diffusive length.

Let us now return to the present flame. At first glance, its reactive zone covers a large domain with a typical length scale proportional to the instantaneous radius. Because the reactive zone contains a large domain in near-equilibrium, let us focus our attention to the transition zone in non-equilibrium mentioned above. As the latter zone corresponds to the locus where the major heat release occurs, we will define l_R as the width at half height of the net heat production rate profile. In our case, it separates a frozen zone from a zone in near-equilibrium as studied by Peters [26], whereas in the simplified model mentioned above it separates two zones in equilibrium [25].

A detailed study of the variation of l_R with respect to the droplet radius reveals a dependency different from that given by Eq. 5. As a result we have plotted in Fig. 16 $\log_{10} l_R$ as a function of $-\log_{10} a$. This figure shows that after a transient regime, a linear relation seems to exist. It approximately corresponds to $l_R = 1.58\ 10^{-3}\ a^{1/2}$ (with l_R and a in cm). We have tried to put forward other couplings between both intrinsic lengths by studying during the droplet lifetime the following quantities: $r_R - a$, $r_T - a$, where r_R denotes the position of the heat release peak and r_T is the position of the maximum of the temperature profile. After a transient period, both quantities are found to approximately behave proportionally to $a^{1/2}$. This proves that the quasi-steady solution does not rigorously exist and, although the chemistry is fast, the reaction produces a coupling with the droplet radius yielding l_R, a new length scale that we can define as

$$\frac{l_R}{a} \approx \left(\frac{e}{a}\right)^{1/2} \tag{7}$$

The relatively simple picture, that we have presented in this paragraph, was found valid as long as the droplet radius is sufficiently large, roughly speaking for droplet radii above 10 μm. For smaller radii, l_R and a are no longer well-separated. This is the source of a reactive picture much more complex than the one given by Fig. 14.

COMPLEMENTARY RESULTS

In this section we briefly present the influence of some parameters on combustion time. As stated before, *the combustion time is defined as the time needed for the oxygen mass to vanish.* More precisely, the parameters considered now are initial droplet radius, ambient pressure,

ambient temperature, ambient composition. As mentioned before, the transport coefficients used correspond to those of ideal gases, and their use is questionable in the dense liquid-like phase. The incidence of this simplification on combustion time and flame structure is finally evaluated through a typical example.

Influence of Initial Droplet Radius

In a vaporization process without combustion, the initial droplet radius is obviously the unique length scale of the problem so that, the process being controlled by diffusion, Dimensional Analysis leads to a vaporization time proportional to the square of the initial droplet radius. Because combustion introduces an additional intrinsic length scale (the reactive-diffusive one), it is relevant to study the effect of the initial droplet radius in typical conditions.

This influence on combustion time is illustrated with Table 4 (the ambience is pure hydrogen at 1500 K and 100 bars).

The combustion time can thus be considered as proportional to the radius squared, despite the existence of the intrinsic diffusive-reactive length scale already mentioned. This shows again that the rate of the process is determined (to the dominant order) by the chemical near-equilibrium rate which is controlled by diffusion on the largest length scale.

On the other hand, when the initial droplet radius becomes of the same order than the reactive-diffusive length scale (say $a_0 \sim 1$ μm), the ignition delay can no more be negligible compared to combustion time, so that this proportionality is no longer valid.

Influence of Ambient Temperature

The ambient temperature during the combustion process has an obvious effect on the flame temperature. In the homogeneous case this effect is feeble as illustrated in Fig. 1 and it remains weak in the non-homogeneous case. A more important influence of the ambient temperature has been already mentioned: the strong dependency of the induction delay. As long as this delay remains much smaller than the droplet lifetime, no sensitive effect is observed. So that, in order to stress this effect, we have to consider small droplets. This is illustrated on Table 5 where the combustion time of a 5 μm radius droplet burning in a pure hydrogen environment at 100 bars is reported: These figures show that above 1500 K no effects are noticeable and confirm that for small droplets the induction delay plays a dominant role at low temperature on the droplet burning time.

TABLE 4

Initial droplet radius a_0 (μm)	5	10	25	50
Combustion time τ (ms)	0.012	0.045	0.28	1.1
Combustion constant $K = a_0^2/\tau$ (cm^2/s)	0.021	0.022	0.022	0.023

Influence of Ambient Pressure

The combustion time was found almost independent of pressure. A very small increase with pressure is actually noticed: for example, a 50-μm radius droplet, burning in an ambience of pure hydrogen at 1500 K, has a combustion time which increases by less than 4% when the pressure is raised from 100 to 200 bars. This behavior has to be related to experimental observations by Faeth et al. [1] and Sato et al. [7] showing hydrocarbon droplets lifetime as a weakly increasing function of pressure in the supercritical combustion regime.

Influence of Ambient Composition

The influence of ambient composition on combustion time is illustrated with the following figures (the ambiance is hydrogen + H_2O vapor at 1500 K and 100 bars, initial droplet radius is $a_0 = 50$ μm).

The increase of combustion time with XH_2O_∞ is due to the decrease of the peak temperature and the shift of its location away from the droplet ([27]–[28]). The last row of Table 6 proves that the combustion time is strongly

TABLE 5

Ambient temperature T_∞ (K):	1300	1400	1500	2500
Combustion time τ (μs):	18.0	13.5	11.9	11.2

TABLE 6

Ambient composition XH_2O_∞ (mole fraction)	0	0.25	0.5	0.75
Combustion time τ (ms)	1.1	1.5	2.2	4.1
Peak temperature (K)	4250	3800	3500	3000
location of the peak temperature (K) (distance from the droplet, reduced by the instant. droplet radius at half combustion time)	1.6	2.0	2.5	3.8
γ: mean T-gradient (between the flame and the interface) (arbitrary unit)	2.6	1.85	1.36	0.76
$\tau\gamma$: mean gradient multiplied by combustion time (arbitrary unit)	2.8	2.8	3.0	3.1

related to the mean gradients between the droplet and the maximum temperature location.

Incidence of Transport Coefficients in the Dense Phase

The calculations above were carried out with the heat capacities, mixture conductivities, and diffusion coefficients being those of ideal gases. This has the nice feature of ensuring the continuity of those coefficients throughout the domain, especially at the "interface." Nevertheless, this use is certainly incorrect in the dense phase where the transport properties should be close to those of a liquid.

Up to now, the mass diffusivity that we have used is largely overestimated (the mass diffusivity in liquids being much smaller than in gases). Furthermore, the ratio λ/c_p of heat conductivity over heat capacity used in the calculation, is certainly underestimated in the dense region. If we assume that the dense fluid is pure oxygen, comparison with experimental data for liquid oxygen shows that the underestimate is large, close to a factor 10.

Thus, it is imperative to check the influence of these large errors in transport coefficients. We have carried out several tests on a typical case: a droplet with an initial radius of 50 μm burning in pure hydrogen at 100 bars and 1500 K. In order to make the transport coefficients more realistic in the dense phase, we have decided to artificially modify them in the dense zone which corresponds more or less to temperatures less than 200 K:

—1st case: only λ/c_p is increased by factor 10 in the dense zone ($T < 200$ K)
—2nd case: only mass diffusivities are decreased by factor 10 ($T < 200$ K)
—3rd case: both previous cases simultaneously.

The effects on combustion time are estimated by comparing to the standard case (Fig. 8) and are reported in Table 7. We observe that the incidence is weak and lies within 7% error. An additional test has been carried out by modifying the definition of the dense zone: $T < 400$ K.

This typical example shows that the combustion time is not sensitive to the transport properties of the dense phase. As noticed in the previous paragraph, this confirms that the data concerning the combustion time appear to be related to some averaged value of the gradients between the flame and the droplet.

Additionally, this test proves that a more sophisticated modeling of the transport properties in the dense region is not required from the quantitative point of view.

Finally, as already mentioned, the weak sensitivity of droplet lifetime to the dense phase transport properties is in complete agreement with the expression of the combustion time yielded by the analytical study by Sanchez-Tarifa et al. [10], and with the sensitivity analysis by Curtis et al. [16].

CONCLUSION

We have carried out a numerical study of the supercritical combustion of a LOX droplet in a stagnant environment of hot hydrogen. The

TABLE 7

Definition of the dense zone	$T < 200$ K	$T < 400$ K
Standard case (no modification)	1.1 ms	1.1 ms
1st case (λ/c_p multiplied by 10 in the dense zone)	1.08 ms	1.08 ms
2nd case (mass diffusivities divided by 10 in the dense zone)	1.18 ms	1.19 ms
3rd case (1st and 2nd case simultaneously in the dense zone)	1.11 ms	1.09 ms

originality of the present work lies in the use of a detailed chemistry model, which enabled us to devote a special attention to ignition process and diffusion flame structure.

We have shown that the ignition process first consists, as classically expected, of the propagation of a premixed flame. This is initiated in the H_2-rich hot side and corresponds to an actual reactive-diffusive deflagration wave. In addition, when the initial droplet radius is sufficiently small ignition is delayed and droplets with diameter less than 1 μm are found to vaporize before burning.

After ignition, a quasi-steady-like diffusion flame is then established. In this regime we observe that the D^2 law is approximately valid. In contrast to the case of a single irreversible reaction, a full chemistry model leads to a very thick flame. Two well-defined reactive zones have been identified:

—a large near-equilibrium zone characterized by net consumption rates which are several order of magnitude lower than the rates of each direct or reverse elementary reactions. The net rates are controlled by diffusion.
—a thin non-equilibrium zone which separates the former zone from the frozen fluid close to the droplet. Although the net chemical rates are here lower than those of the former zone as illustrated by Fig. 14 (because the temperature is lower), the net chemical rates are not negligible compared to those of the direct reaction. Furthermore, the length scale of the latter region is found to behave as the square root of the instantaneous droplet radius and a detailed analysis shows that just two elementary reactions are involved in this zone.

Then, the influence of the parameters of the combustion chamber has been considered. In particular the combustion time is found almost independent of pressure, and influence of initial droplet radius confirms that droplet combustion is a diffusion controlled process.

The authors are grateful to Professor A. Linan for encouraging and extremely helpful discussions. This work has received the support of the "Programme de Recherches Coordonnées CNRS/CNES/SEP: Combustion dans les moteurs-fusées."

APPENDIX: O_2–H_2O VAPOR-LIQUID PHASE EQUILIBRIA

In the classical flame sheet model, or in the model of one irreversible fast chemical reaction, the droplet is only surrounded by combustion products. Thus, in the first approximation corresponding to these models, we should treat the interface by seeking for the vapor–liquid coexistence in a O_2–H_2O mixture. This appendix presents the results that one obtains when studying this liquid-vapor binary mixture at high pressure. The details of the method can be found in Refs. 12 and 13. It consists of determining for a given pressure and temperature of the O_2–H_2O binary system, the composition and the molar volume of the liquid and vapor phases. Four unknowns are present and the corresponding equations express that the application of the equation of state in each phase yields the prescribed pressure, and that each component has the same chemical potential (or fugacity) in both phases. The Redlich–Kwong–Soave equation of state is used for estimating the chemical potentials and the set of equations is solved iteratively using a Newton iterative method. The main results of the calculations are summarized in Fig. 17a in the T-P diagram. This figure can be summarized as follows:

—First we have to look for solutions in which the liquid phase, initially of pure oxygen, accepts solubility of the ambient gas at low temperature. Such a solution is possible only as a very narrow perturbation of the pure O_2 liquid–vapor equilibrium. In other words, just traces of water are present in the mixture in both phases. This type of solution does no longer exist above 54 bars. Let us describe the solutions obtained at 53 bars. the temperature range where these solutions exist is between T_{min} = 156.32 K and T_{max} = 156.37 K. All solutions have corresponding oxygen mole fractions in the two phases greater than 99% (i.e., feeble perturbation of the pure oxygen liquid–vapor equilibrium). T_{min} corresponds to the critical

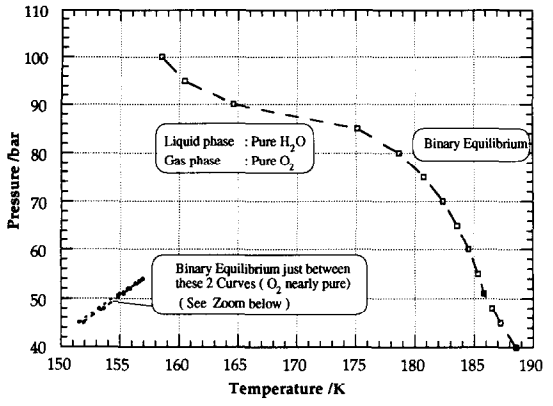

(a)

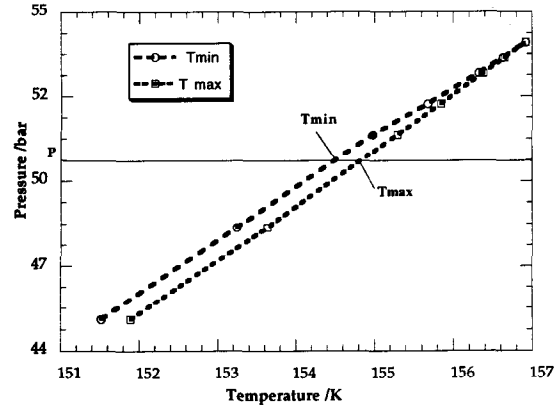

(b)

Fig. 17. (a) Domain of existence of liquid-vapor equilibria for the binary mixture O_2-H_2O (cf. Appendix). (b) Zoom of (a) near O_2 saturation curve. This figure represents the minimum and maximum temperatures where a binary O_2-H_2O equilibrium (with a dominant presence of oxygen) can be calculated.

mixing point where the two phases compositions and densities become equal. The curve T_{min} versus P can thus be considered in the T-P diagram as the critical line. On the other hand, T_{max} is the temperature beyond which we could not find any solution. The band T_{min}–T_{max} decreases with increasing pressure and vanishes at P close to 54 bars. This is illustrated in Figure 17b which is a blowup of Fig. 17a.

—Far from the pure O_2 liquid-vapor equilibrium curve, a strongly different solution is obtained where the liquid phase is quasi-pure water. For example, at $P = 53$ bars and $T = 429.2$ K, the oxygen mole fraction in the liquid is less than 0.1% and in the gas greater than 87%. The locii where the equilibrium involves a significant mixture in the gas phase, lie above the dashed line on Fig. 17a. Below this line, this solution tends to a liquid phase with no oxygen, and a vapor phase with no water. For our purpose (i.e., phase equilibrium at the LOX droplet interface) this solution is of course out of interest.

In conclusion we find ourselves constrained to refuse the latter equilibrium and to point out that above 54 bars no liquid–vapor equilibrium exists when H_2O–O_2 mixture is involved. It is worth noting that partially similar conclusions were drawn in Ref. 3 where the authors outline that the ternary equilibrium H_2O–O_2–H_2 is only possible in the sense of a very weak perturbation of the binary O_2–H_2 equilibrium.

REFERENCES

1. Faeth, G. M., Dominicis, D. P., Tulpinski, J. F., and Olson, D. R., *Twelfth Symposium (International) on Combustion*, The Combustion Institute, Pittsburgh, 1962 p. 9.
2. Rosner, D. E., and Chang, W. S., *Combust. Sci. Technol.* 7:145–158, (1973).
3. Litchford, J., and Jeng, San-Mou., AIAA/SAE/ASME/ASEE Paper 90-219, 26th Joint Propulsion Conference, Orlando, July 16–18, 1990.
4. Yang, V., Lin, N. N., and Shuen J. S., 30th Aerospace Sciences Meeting, AIAA, Paper 92-0103 (1992).
5. Shuen, J. S., Yang, V., and Hsiao, C. C., *Combust. Flame* 89: 299–319 (1992).
6. Nicoli, C., Haldenwang, P., and Daou, J., in preparation.
7. Sato, J., Tshe, M., Niwa, M., and Kono, M., *Combust. Flame* 82: 142–150 (1990).
8. Spalding, D. B., *ARS J.* 29:828–835 (1959).
9. Rosner, D. E., *AIAA J.* 5:163–166 (1967).
10. Sanchez-Tarifa, C., Crespo. A., and Fraga, E., *Astronaut. Acta* 17:685–692 (1972).
11. Mass, U., and Warnatz, J., *Combust. Flame* 74:53 (1988).
12. Reid, R. C., Prausnitz, J. M., and Poling, B. E., *The Properties of Gases and Liquids*, 4th ed., McGraw-Hill, New York, 1987.
13. Wallas, S. M., *Phase Equilibria in Chemical Engineering*, Butterworth, 1985.
14. Kee, R. J., Miller, J. A., and Jefferson, T. H., SANDIA Report SAND80-8003, 1980.
15. Kee, R. J., Warnatz J., and Miller J. A., SANDIA Report SAND83-8209, 1983.

16. Curtis, E. W., and Farrel, P. V., *Combust. Flame* 90:85 (1992).
17. Patankar, S. V., *Numerical Heat Transfer and Fluid Flow*, McGraw-Hill, New York, 1980.
18. Yanenko, N. N., *The Method of Fractional Steps*, Springer-Verlag, 1971.
19. Hindmarsh, A., *LSODE Livermore Solver for Ordinary Differential Equations*, Lawrence Livermore Laboratory, 1978.
20. Clarke, J. F., *Proc. R. Soc. A* 312:65–83 (1969).
21. Fendell, F., *Astronaut. Acta* 13:183–191 (1967).
22. Linan, A., and Crespo, A., *Combust. Sci. Technol.* 14:95–117 (1976).
23. Daou, J., Gauducheau, J. L., and Haldenwang, P., *Combust. Sci. Technol.* (in press).
24. Zeldovich, Ya. B., Barenblatt, G. I., Librovich, V. B., and Makhviladze, G. M., *The Mathematical Theory of Combustion and Explosions*, Consultants Bureau, New York, 1985.
25 Linan, A., *Acta Astronaut.* 1:1007–1039 (1974).
26. Peters, N., *Int. J. Heat Mass Transf.* 22:691–703 (1978).
27. Godsave, G. A. E., *Fourth Symposium (International) on Combustion*, Williams & Wilkins, Baltimore, 1953, pp. 818–830.
28. Spalding, D. B., *Fourth Symposium (International) on Combustion*, Williams & Wilkins, Baltimore, 1953, pp. 847–864.

Received 23 November 1993; revised 14 July 1994